

Search for long-lived charged particles using the CMS detector in Run-2

Tamas Almos Vami*

^a*University of California Santa Barbara, , Santa Barbara, 93117, CA, USA*

Abstract

Long-lived charged particles are predicted by various theories beyond the Standard Model, leading to unique signatures that could reveal new physics. At the LHC, the CMS detector enables searches for these massive particles, identifiable by their characteristic ionization patterns. Using data collected during 2017-2018, we search for signals of anomalous ionization in the silicon tracker. We present a novel approach to background prediction, utilizing the distinct ionization measurements of the silicon pixel and strip detectors as independent variables. We interpret the results within several models including those with staus, stops, gluinos, and multiply charged particles as well as a new model with decays from a Z' boson.

Keywords: Long-lived, exotic physics, energy loss in silicon, CMS

*On behalf of the CMS Collaboration

1. Introduction

The Standard Model (SM) is a quantum field theory that explains the universe at its fundamental level. Often we describe it by its particle content. The force-carrying particles, known as bosons, mediate fundamental interactions: the photon for electromagnetic interaction, gluons for the strong interaction, and the W and Z bosons for the weak interaction. The Higgs boson, a scalar particle, gives mass to elementary particles through the Higgs mechanism. The remaining particles, called fermions, make up matter and are divided into quarks and leptons. The quarks interact with all the three forces, while the (charged) leptons interact with (electromagnetic and) weak interaction(s). There are three fermion families in the SM.

Despite its many successes, the Standard Model cannot be the ultimate theory of the universe, as it leaves several fundamental questions unanswered. For example, according to the Big Bang theory, equal amounts of matter and antimatter should have been created, yet the observable universe consists almost entirely of matter. What causes this matter-antimatter asymmetry? There is strong evidence of the existence of dark matter, but what the SM does not provide any candidate particle for it. Another puzzle is the hierarchy problem: why is it that the gravity is orders of magnitude weaker than any other force in the SM?

There has been several theoretical attempts to answer these questions. One of the first popular solution was to introduce superpartners to the SM particles [1, 2]: each boson would have a fermion partner, and each fermion would have a boson partner. This model is called Supersymmetry (SUSY) and would answer all the questions above. The partner of the quarks and gluons are the squarks and gluinos, while the partner of the leptons are the sleptons. For example, the SUSY partner of the top quark is the stop squark, and the partner of the tau lepton is the stau slepton. Further theories that answer part of the questions above have been proposed, too. Among them the solution is provided by introducing additional heavy Z' bosons, or a 4th generation of fermions (τ'), or several other Higgs bosons.

These questions and theories have remained open for decades, since no significant experimental evidence for physics beyond the Standard Model (BSM) has been observed to date. The collider searches at the Large Hadron Collider (LHC) and other laboratories have been looking for signatures in which the BSM particles decay promptly. However, there are several mechanisms that can lead to longer lifetime, even in the SM. With this we have a

new direction to explore BSM physics and to look for long-lived particles [3]. In this work, we search for "stable" particles—meaning not necessarily fundamentally stable, but stable on the detector level, where they traverse the detector without decaying. Figure 1 shows a flow chart to categorize how these particles interact with different forces and what models would predict their existence. If they are electrically charged, these particles are often referred to as Heavy Stable Charged Particles (HSCPs) [4, 5, 6, 7].

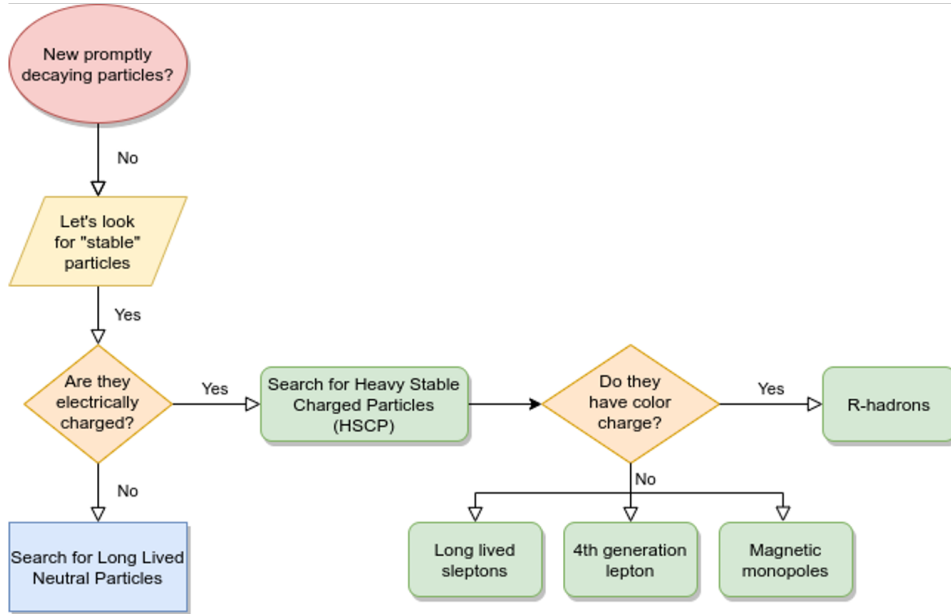


Figure 1: Flow chart for possible new directions in searches.

If the HSCPs have color charge that means they will hadronize. A BSM example for this are the R-hadrons from split-SUSY [8, 9, 10, 11]. R-hadrons are a bound state of SM and SUSY particles. Some of these form negative, neutral, positive, or even double positive hadrons. The R-hadron's interactions with matter is described in the model in Ref. [12, 13]. If the HSCPs are colorless, one can think of several theories that would predict them. For example a magnetic monopole [14], i.e. the magnetic equivalent of an isolated electric charge, would act as an HSCP. However, it would bend differently, and because of that we do not consider it in this work. Sleptons in GGM SUSY [15] are predicted to be long-lived. We consider both pair production and cascade production of staus from GMSB SUSY [16, 17] in this work. Furthermore, 4th generation leptons (τ') are considered too, both

with singly and doubly charge. We consider both pair-production and a production through a boosted Z' boson. This last model is especially interesting, as it was proposed as a solution an excess seen by ATLAS [18].

ATLAS reported a 3 sigma excess with SM compatible v/c (β) [19]. The resolution of this by the phenomenologist was to produce the doubly charged τ' from the decay of a boosted Z' particle. In this scenario the ionization will be high while the β can be high too.

One common aspect of all these models is that they have a distinctively different characteristic ionization loss (dE/dx) from the SM particles. That is why this work presents a signature driven, model independent search with many possible interpretations. The HSCP signature is an isolated track of high p_T with large energy deposits in the tracker (large dE/dx).

This analysis is carried out using the CMS detector at the LHC. A detailed description of the CMS detector, together with a definition of relevant kinematic variables, can be found in Ref. [20]. All figures in this proceedings are part of the results submitted to JHEP with ArXiv ID of 2410.09164 [21], with supplementary material under CMS-EXO-18-002, also available under HEPData [22].

2. Ionization observables

We use four observables in this analysis. Eq. 1 shows a discriminator in the pixel detector, called F_i^{Pixels} , where P'_j is a hit level minimum ionizing particle (MIP) compatibility based on the Tracker Detector Performance Group's detailed calibrations, n is the number of pixel hits (excluding layer 1).

$$F_i^{\text{Pixels}} = 1 - \prod_{j=1}^n P'_j \sum_{k=0}^{n-1} \frac{[-\ln(\prod_{j=1}^n P'_j)]^k}{k!} \quad (1)$$

The calibrations are based on a very detailed simulation called PIXELAV [23]. These include effects like bias voltage changes, gain calibration changes, temperature, and irradiation dose. The electric field map input to PIXELAV is determined using ISE TCAD [24] simulations of a pixel cell. The Lorentz drift vs. substrate depth has been tuned to calibration data. The simulation also includes carrier trapping, diffusion, charge induction on the sensors and noise simulation. The F_i^{Pixels} templates have been produced 25 times over the 2017–2018 period, corresponding to an update about every 5 fb^{-1} .

The second discriminator, using the strip detector, is shown in Eq. 2, where P_j is a hit level MIP probability for a charge to be smaller/equal to the measured charged based on our templates calibrated at low momentum (20-48 GeV) data, N is the number of (cleaned) hits in the strips detector.

$$G_i^{\text{Strips}} = \frac{3}{N} \left(\frac{1}{12N} + \sum_{j=1}^N \left[P_j \left(P_j - \frac{2j-1}{2N} \right)^2 \right] \right) \quad (2)$$

These two quantities are uncorrelated by construction. Figure 2 shows the F_i^{Pixels} vs. G_i^{Strips} distributions for both signal (1800 GeV gluino R-hadron) and background (QCD, W+jet, $t\bar{t}$) simulations. Indeed we can observe that the two quantities are not correlated for background, while they are accumulated in the high end in both quantities for the signal.

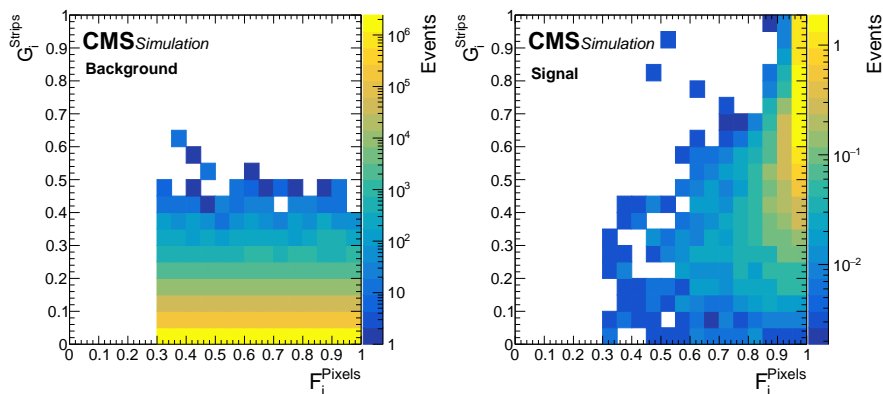


Figure 2: The F_i^{Pixels} vs. G_i^{Strips} distributions for the SM background (QCD, W+jet, $t\bar{t}$) simulation (left), and an 1800 GeV gluino R-hadron simulation (right), for events after pre-selection.

Besides these discriminators, we also use a dE/dx estimator [25] as shown in Eq. 3.

$$I_h = K \frac{m^2}{p^2} + C \quad (3)$$

This uses a squared harmonic mean in order to suppress the tails of the Landau distribution, which happen quite often. This estimate, on the other hand, is sensitive to lower fluctuations. However, those do not happen very often, one example can be a high voltage change on the sensors.

The mass of the HSCP can be interpreted through approximating the Bethe–Bloch formula with $I_h(m, p, K, C)$, where the empirical parameters K and C are determined using a sample of low-momentum particles composed of protons, kaons and pions. The calibrated value of these parameters are $K = 2.5 \pm 0.01$ MeV/cm and $C = 3.14 \pm 0.01$ MeV/cm.

The distribution of I_h vs. HSCP candidate p can be seen in Fig. 3 for different signal simulations in colors and for data as a histogram. The dashed lines represent the distribution for a particle with a mass of 557 and 2000 GeV on the left, and 1400 and 3000 GeV on the right. These are based on Eq. 3.

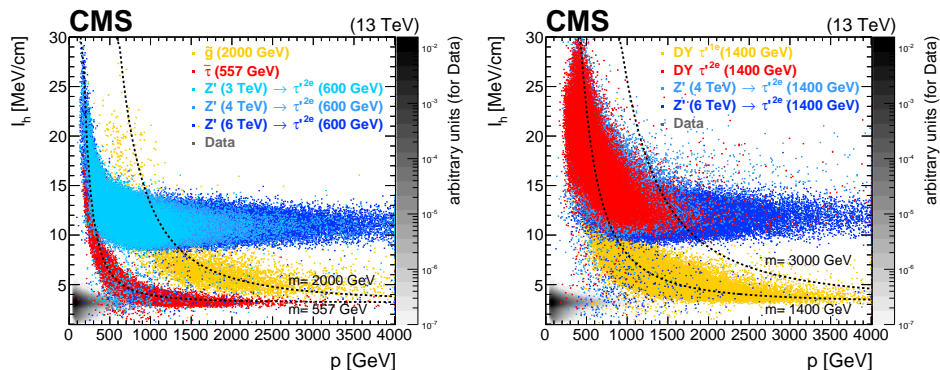


Figure 3: The distribution of I_h vs. HSCP candidate p . Different colors correspond to different signal simulations. Data is shown in a grey histogram, normalized to unit area. Based on Eq. 3 we show the distribution for a particle mass of 557 and 2000 GeV on the left, and 1400 and 3000 GeV on the right using the dashed lines.

3. Understanding the background and preselection

We used Monte Carlo (MC) SM simulations to understand our background. From these studies we concluded the following list of sources:

- Fake tracks
- Bad ionization measurement
- Being in the tail of the Landau distribution
- Overlapping tracks in the tracker coming from
 - Pileup

- Boosted mesons decays to overlapping dileptons
- Tracks in the core of jets

Fig. 4 shows an example in MC where a boosted J/Ψ particle is created and decays to two muons, that are overlapping in the tracker and they are also very close in the muon chambers.

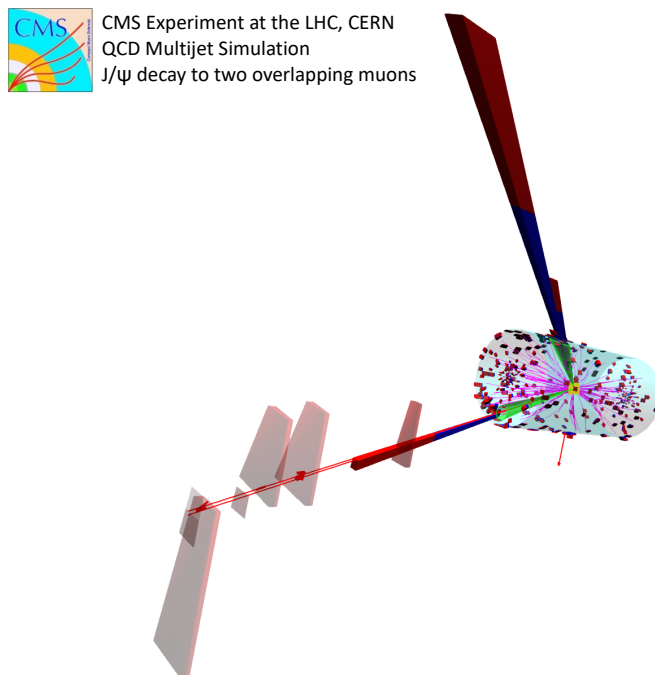


Figure 4: Event display of a boosted J/Ψ particle decaying into two overlapping muons.

With this understanding we optimize our preselection. We used 2017–2018 data corresponding to 101 fb^{-1} data. Exclusion of 2016 data is motivated by the read-out chip issues in the strips detector and having the Phase-0 pixel detector [26]. The cutflow after applying each preselection cut is shown in Table 1. The details of these tracking criteria are explained in Ref. [27].

The definition of the relative isolation [28] is in Eq. 4.:

$$I_{\text{PF}}^{\text{rel}} = \frac{(\sum_{\Delta R < \Delta R_{\text{mini-iso}}} p_{\text{T}}^{\text{PF}}) - p_{\text{T}}^{\text{HSCP}}}{p_{\text{T}}^{\text{HSCP}}}, \quad (4)$$

| Selection criteria | Data | gluino (1.8 TeV) | stau (557 GeV) |
|---|-------|------------------|----------------|
| All events | 1 | 1 | 1 |
| Trigger | 0.15 | 0.11 | 0.86 |
| $p_T > 55 \text{ GeV}$ | 0.11 | 0.11 | 0.86 |
| $ \eta < 1$ | 0.059 | 0.074 | 0.64 |
| # of valid pixel hits in L2-L4 ≥ 2 | 0.056 | 0.071 | 0.62 |
| Fraction of valid hits > 0.8 | 0.052 | 0.069 | 0.62 |
| # of dE/dx measurements ≥ 10 | 0.052 | 0.069 | 0.62 |
| High-purity track | 0.052 | 0.069 | 0.62 |
| Track $\chi^2/\text{dof} < 5$ | 0.052 | 0.069 | 0.62 |
| $d_z < 0.1 \text{ cm}$ | 0.052 | 0.069 | 0.62 |
| $d_{xy} < 0.02 \text{ cm}$ | 0.048 | 0.069 | 0.62 |
| $I_{\text{PF}}^{\text{rel}} < 0.02$ | 0.014 | 0.065 | 0.61 |
| $I_{\text{trk}} < 15 \text{ GeV}$ | 0.014 | 0.065 | 0.61 |
| PF $E/p < 0.3$ | 0.014 | 0.064 | 0.61 |
| $\sigma_{p_T}/p_T^2 < 0.0008$ | 0.014 | 0.064 | 0.61 |
| $F_i^{\text{Pixels}} > 0.3$ | 0.011 | 0.064 | 0.60 |

Table 1: Cumulative selection efficiency for the data and for two signal hypotheses.

where

$$\Delta R_{\text{mini-iso}} = \begin{cases} 0.2, & p_T^{\text{HSCP}} < 50 \text{ GeV} \\ 10 \text{ GeV}/p_T^{\text{HSCP}}, & 50 \text{ GeV} < p_T^{\text{HSCP}} < 200 \text{ GeV} \\ 0.05, & p_T^{\text{HSCP}} > 200 \text{ GeV}. \end{cases}$$

The definition of the tracker-based isolation is shown in Eq. 5.

$$I_{\text{trk}} = \left(\sum_{\Delta R < \Delta R_{\text{mini-iso}}} p_T^{\text{trk}} \right) - p_T^{\text{HSCP}} \quad (5)$$

Preselection cuts are ensuring a clean track environment, homogeneous sensor technology, they remove damaged clusters, pileup, and overlaying tracks, e.g. from boosted meson decays (J/Ψ) as mentioned earlier.

For the trigger choice we decided to use a single muon trigger. This is motivated by the ATLAS excess being compatible with muons and also leads to less QCD and more electroweak processes as background.

Figure 5 shows the trigger efficiency binned in pseudorapidity ranges for gluinos (left) and staus (right). We can clearly see that this trigger choice is

more efficient for muon-like signal like the staus and the τ' particles. However, we still are able to trigger on the R-hadrons, too. We can also observed that the barrel detector, displayed with blue curves, has higher efficiency.

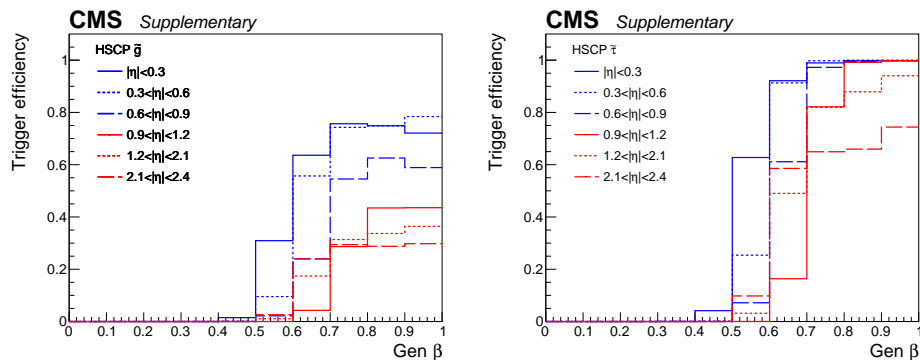


Figure 5: Trigger efficiency as a function of generated β for gluino (left) and stau (right) in bins of pseudorapidity.

4. Data-driven background prediction

We use two independent methods for background prediction in this analysis, which together provide an additional handle, especially in light of the ATLAS excess. Both of them are data driven, and reuse the trigger selection, preselection, and signal systematics. The first method is referred as the ionization method. This is a new approach, relying on independence of the pixel detector and strip detector [25, 27], it uses a transfer function and invokes a shape based analysis. The second one is the mass method. This is the improved historical approach [29, 30, 31, 32], assuming the independence of I_h and p as well as the G_i^{Strips} and p_T as a counting experiment in a dedicated mass window. In this proceedings, we concentrates on the ionization method for simplicity.

The ionization method is a fully data driven method relying on the independence of the pixels and strips detectors. The F_i^{Pixels} variable spans the PASS ($F_i^{\text{Pixels}} > 0.9$) and FAIL regions ($0.9 > F_i^{\text{Pixels}} > 0.3$). We perform a simultaneous fit in bins of the G_i^{Strips} distribution using the full G_i^{Strips} shape. The background yield in j -th bin of the G_i^{Strips} distribution in the PASS region is determined using Eq. 6, where $N_{\text{FAIL}}^{\text{bkg}}(j)$ is a freely floating parameter that determines the background yield in the j -th bin, which is constrained

to values close to the observed data yield during the fit, and $R_{P/F}(j)$ is the value of the pass-to-fail ratio for bin j .

$$N_{\text{PASS}}^{\text{bkg}}(j) = R_{P/F}(j) N_{\text{FAIL}}^{\text{bkg}}(j) \quad (6)$$

We used a constant $R_{P/F}$ across the bins j . Higher-order polynomials were tested using Fisher's F -test [33, 34] and did not provide significantly better results as the constant function. We choose the binning of the G_i^{Strips} distribution so the last bin contains $\mathcal{O}(1)$ event in the FAIL region for the data.

We defined two control regions, one with $50 < p_T < 55$ GeV and $55 < p_T < 200$ GeV. The background prediction performs very well in these regions, Fig. 6 shows the control region for $55 < p_T < 200$ GeV, left being the FAIL and right the PASS region.

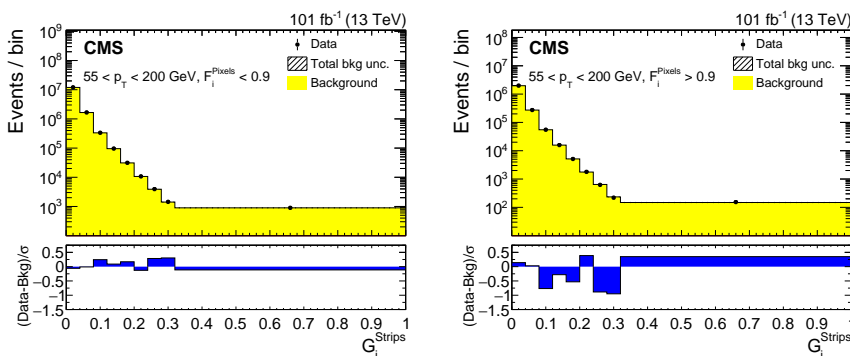


Figure 6: Control region with $55 < p_T < 200$ GeV, showing the FAIL region in the left and the PASS region in the right.

5. Results

Given that the the background prediction performs well in the control region, we can look at the signal region next. This is defined as $p_T > 200$ GeV, $F_i^{\text{Pixels}} > 0.9$ and the full shape of G_i^{Strips} is used. Figure 7 shows the signal region for FAIL (left) and PASS (right). The results are consistent with the SM. In the last bin we observe one event, where 0.4 ± 0.2 were expected. The bin before one event was expected and zero is observed.

The visualization of the "excess" event above can be seen in Fig. 8 (left). It has $G_i^{\text{Strips}} = 0.43$ and $F_i^{\text{Pixels}} = 0.96$ and the $I_h = 5.35$ MeV/cm. The mass

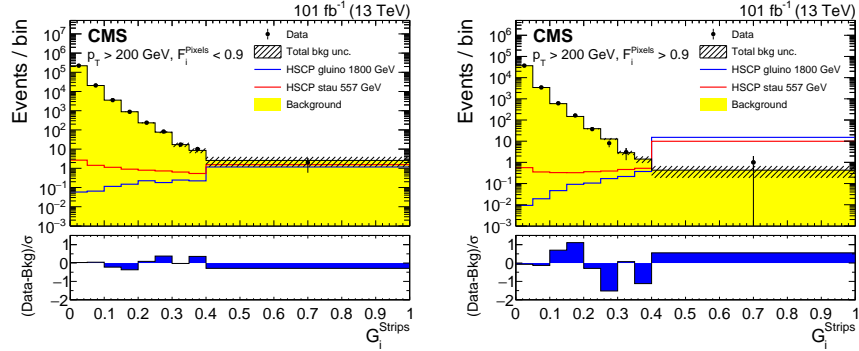


Figure 7: Signal region with $p_T > 200$ GeV, $F_1^{\text{Pixels}} > 0.9$, left is FAIL and right is PASS. The results are consistent with the SM.

corresponding to this candidate is 198 GeV. For illustration purposes, we also show a simulated gluino R-hadron event in the right.

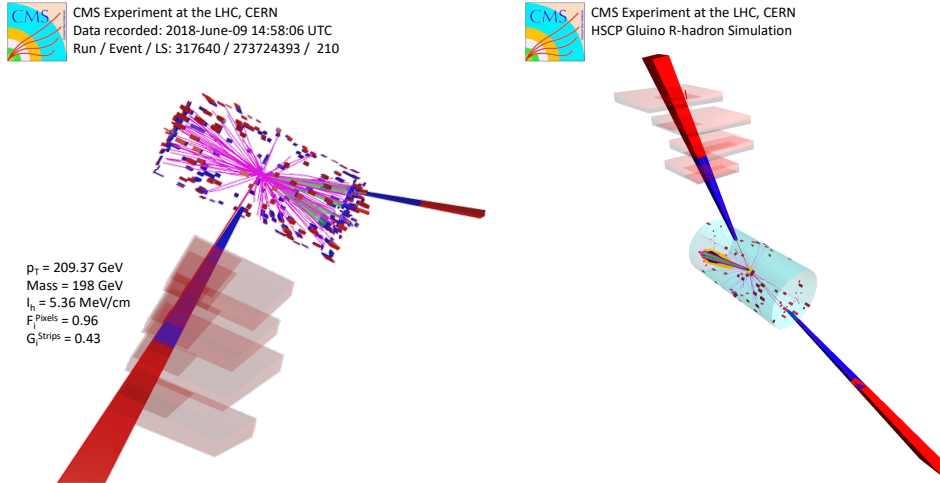


Figure 8: Visualization of the "excess" event (left) and a simulated gluino R-hadron event (right).

Given that no significant excess beyond the SM is observed, we set limits on a variety of signal models. The full CLs method [35, 36] is used as test statistic [37] and using a lognormal model for nuisance parameters affecting yields. The CMS COMBINE tool is used to perform the statistical analysis [38].

Figure 9 shows the exclusion limits for gluino R-hadrons (left) and stop R-hadrons (right). The observed (expected) mass limits for ionization method are 2.06 (2.06) TeV for the gluino and 1.40 (1.43) TeV for the stop. The uncertainty bands are assymetric since we are in the low background case where downward fluctuations reach zero already.

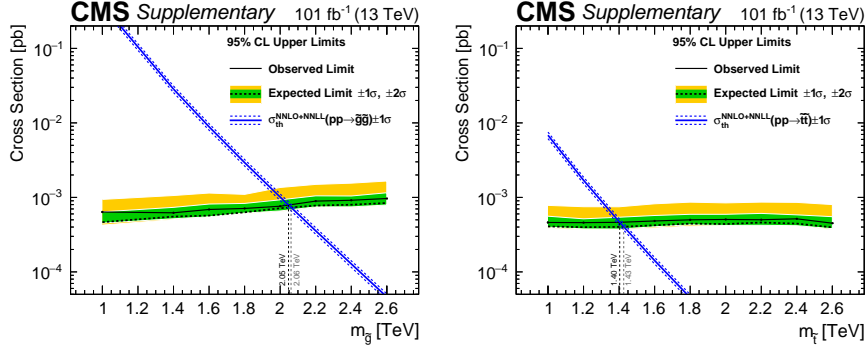


Figure 9: Exclusion limits for gluino R-hadrons (left) and stop R-hadrons (right).

Figure 10 shows the exclusion limits for pair-produced stau with different handedness (left) and for GMSB produced stau (right).

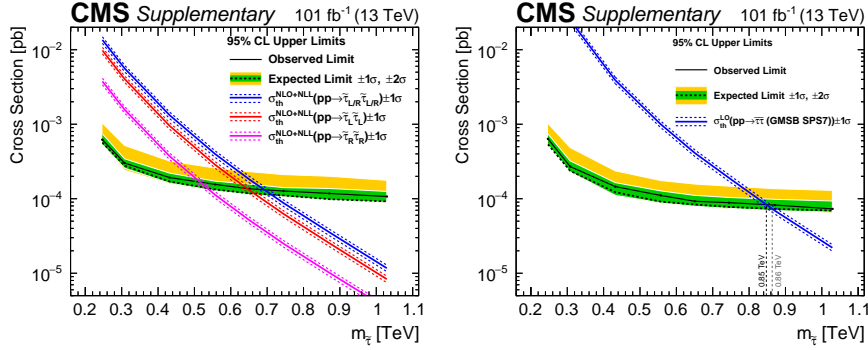


Figure 10: Exclusion limits for pair-produced stau (left) and GMSB produced stau (right).

Figure 11 shows the exclusion limits for pair-produced τ' with 1e charge (left) and with 2e charge (right).

Figure 12 shows the exclusion limits for Z' -produced τ' with 1e charge (left) and with 2e charge (right).

The mass method [31] inverts Eq. 3 to calculate the mass [32] and performs a counting experiment in a mass windows for each interpretation and

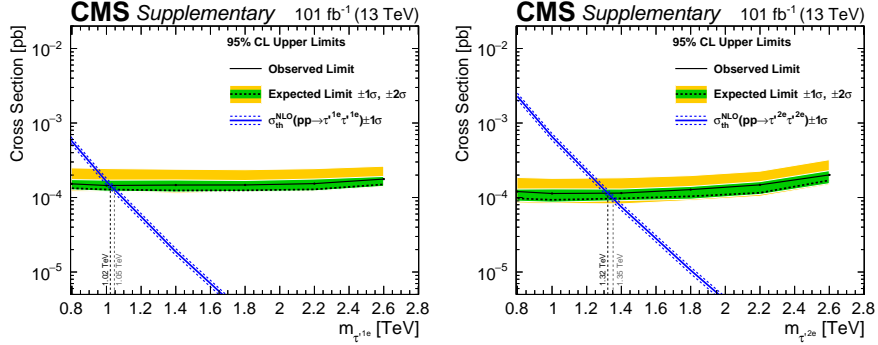


Figure 11: Exclusion limits for pair-produced stau (left) and GMSB produced stau (right).

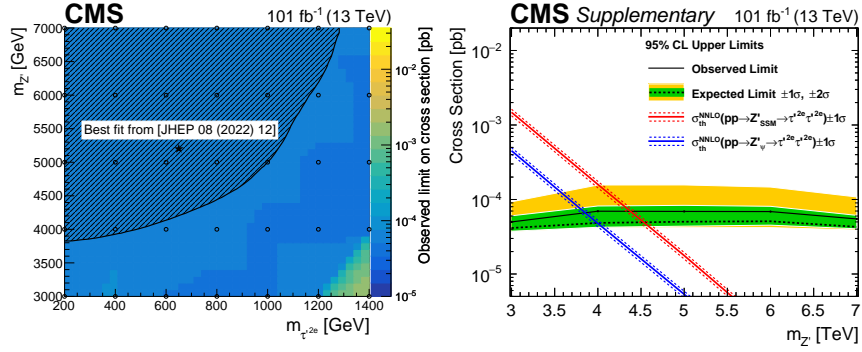


Figure 12: Exclusion limits for pair-produced stau (left) and GMSB produced stau (right).

mass point. The full description of the method can be found in Ref. [21]. Table 2 is the executive summary showing the expected and observed mass limits for various HSCP interpretations including both background estimate methods. The two methods show similar sensitivity. The single excess event in the ionization method makes the observed limits weaker, while for the case of the mass method there was no excess so the observed limit is in line with the expected one.

6. Conclusions

A signature based, model independent search for HSCPs has been presented. The background was studied with MC samples, and the preselection was optimized to remove both physically motivated highly ionizing SM processes together with mismeasured tracks. Two methods of data-driven

| Model | Ionization method | | Mass method | |
|-----------------------------------|-------------------|------------|-----------------|------------|
| | Exp. (TeV) | Obs. (TeV) | Exp. (TeV) | Obs. (TeV) |
| gluino | 2.06 ± 0.06 | 2.06 | 2.08 ± 0.02 | 2.08 |
| stop | 1.43 ± 0.05 | 1.40 | 1.47 ± 0.02 | 1.47 |
| GMSB SPS7 stau | 0.86 ± 0.07 | 0.85 | 0.87 ± 0.05 | 0.85 |
| pair-prod. stau-R | 0.53 ± 0.03 | 0.52 | 0.50 ± 0.07 | 0.51 |
| pair-prod. stau-L | 0.66 ± 0.04 | 0.64 | 0.67 ± 0.06 | 0.61 |
| pair-prod. stau-L/R | 0.71 ± 0.04 | 0.69 | 0.75 ± 0.08 | 0.64 |
| DY-prod τ' ($Q = 1e$) | 1.05 ± 0.05 | 1.02 | 1.14 ± 0.03 | 1.14 |
| DY-prod τ' ($Q = 2e$) | 1.35 ± 0.05 | 1.32 | 1.41 ± 0.02 | 1.41 |
| $Z'_{Phi} \rightarrow \tau'\tau'$ | 3.99 ± 0.21 | 3.95 | 4.03 ± 0.01 | 4.03 |
| $Z'_{SSM} \rightarrow \tau'\tau'$ | 4.53 ± 0.23 | 4.38 | 4.56 ± 0.01 | 4.57 |

Table 2: Expected and observed mass limits for various HSCP interpretations including both background estimate methods.

background predictions were developed. A novel approach relying on the independence of the ionization in the tracking detectors and an improved version of the historical mass method. This proceedings concentrates on the ionization method and includes the mass results for completeness. No significant excess over the SM expectation was found. The results were interpreted in 10 different models, one of them is a direct response to an excess seen by ATLAS. With this the mass exclusion limits are best published to date.

References

- [1] C. W. Bauer, Z. Ligeti, M. Schmaltz, J. Thaler, D. G. E. Walker, Supermodels for early LHC, Phys. Lett. B 690 (2010) 280. [arXiv:0909.5213](#), [doi:10.1016/j.physletb.2010.05.032](#).
- [2] A. Kusenko, M. E. Shaposhnikov, Supersymmetric Q-balls as dark matter, Phys. Lett. B 418 (1998) 46. [arXiv:hep-ph/9709492](#), [doi:10.1016/S0370-2693\(97\)01375-0](#).
- [3] L. Lee, C. Ohm, A. Soffer, T.-T. Yu, Collider searches for long-lived particles beyond the Standard Model, Prog. Part. Nucl. Phys. 106 (2019) 210. [arXiv:1810.12602](#), [doi:{10.1016/j.ppnp.2019.02.006}](#).

- [4] M. Drees, X. Tata, Signals for heavy exotics at hadron colliders and supercolliders, *Phys. Lett. B* 252 (1990) 695. doi:10.1016/0370-2693(90)90508-4.
- [5] M. Fairbairn, A. C. Kraan, D. A. Milstead, T. Sjöstrand, P. Z. Skands, T. Sloan, Stable massive particles at colliders, *Phys. Rept.* 438 (2007) 1. arXiv:hep-ph/0611040, doi:10.1016/j.physrep.2006.10.002.
- [6] B. Koch, M. Bleicher, H. Stoecker, Black holes at LHC?, *J. Phys. G* 34 (2007) S535. arXiv:hep-ph/0702187, doi:10.1088/0954-3899/34/8/S44.
- [7] D. Fargion, M. Khlopov, C. A. Stephan, Cold dark matter by heavy double charged leptons?, *Class. Quant. Grav.* 23 (2006) 7305. arXiv:astro-ph/0511789, doi:10.1088/0264-9381/23/24/008.
- [8] G. F. Giudice, A. Romanino, Split supersymmetry, *Nucl. Phys. B* 699 (2004) 65. arXiv:hep-ph/0406088, doi:10.1016/j.nuclphysb.2004.11.048.
- [9] N. Arkani-Hamed, S. Dimopoulos, G. F. Giudice, A. Romanino, Aspects of split supersymmetry, *Nucl. Phys. B* 709 (2005) 3. arXiv:hep-ph/0409232, doi:10.1016/j.nuclphysb.2004.12.026.
- [10] J. L. Hewett, B. Lillie, M. Masip, T. G. Rizzo, Signatures of long-lived gluinos in split supersymmetry, *JHEP* 09 (2004) 070. arXiv:hep-ph/0408248, doi:10.1088/1126-6708/2004/09/070.
- [11] W. Kilian, T. Plehn, P. Richardson, E. Schmidt, Split supersymmetry at colliders, *Eur. Phys. J. C* 39 (2005) 229. arXiv:hep-ph/0408088, doi:10.1140/epjc/s2004-02046-5.
- [12] A. C. Kraan, Interactions of heavy stable hadronizing particles, *Eur. Phys. J. C* 37 (2004) 91. arXiv:hep-ex/0404001, doi:10.1140/epjc/s2004-01997-7.
- [13] R. Mackeprang, A. Rizzi, Interactions of coloured heavy stable particles in matter, *Eur. Phys. J. C* 50 (2007) 353. arXiv:hep-ph/0612161, doi:10.1140/epjc/s10052-007-0252-4.

- [14] J. S. Schwinger, Magnetic charge and quantum field theory, *Phys. Rev.* 144 (1966) 1087. doi:10.1103/PhysRev.144.1087.
- [15] P. Meade, N. Seiberg, D. Shih, General gauge mediation, *Prog. Theor. Phys. Suppl.* 177 (2009) 143. arXiv:0801.3278, doi:10.1143/ptps.177.143.
- [16] G. F. Giudice, R. Rattazzi, Theories with gauge mediated supersymmetry breaking, *Phys. Rept.* 322 (1999) 419. arXiv:hep-ph/9801271, doi:10.1016/S0370-1573(99)00042-3.
- [17] B. C. Allanach, et al., The Snowmass points and slopes: Benchmarks for SUSY searches, *Eur. Phys. J. C* 25 (2002) 113. arXiv:hep-ph/0202233, doi:10.1007/s10052-002-0949-3.
- [18] G. F. Giudice, M. McCullough, D. Teresi, dE/dx from boosted long-lived particles, *JHEP* 08 (2022) 012. arXiv:2205.04473, doi:10.1007/jhep08(2022)012.
- [19] ATLAS Collaboration, Search for heavy, long-lived, charged particles with large ionisation energy loss in pp collisions at $\sqrt{s} = 13$ TeV using the ATLAS experiment and the full Run 2 dataset, *JHEP* 06 (2023) 158. arXiv:2205.06013, doi:10.1007/JHEP06(2023)158.
- [20] CMS Collaboration, The CMS experiment at the CERN LHC, *JINST* 3 (2008) S08004. doi:10.1088/1748-0221/3/08/S08004.
- [21] CMS Collaboration, Search for heavy long-lived charged particles with large ionization energy loss in proton-proton collisions at $\sqrt{s} = 13$ TeV, *JHEP* (2024). arXiv:2410.09164.
- [22] CMS Collaboration, HEPData record for this analysis (2024). doi:10.17182/hepdata.153850.
- [23] V. Chiochia, et al., Simulation of the CMS prototype silicon pixel sensors and comparison with test beam measurements, *IEEE Trans. Nucl. Sci.* 52 (2005) 1067. arXiv:physics/0411143, doi:10.1109/TNS.2005.852748.
- [24] ISE Engineering, ISE TCAD Release 9.0, ISE Integrated Systems Engineering AG, Zürich, Switzerland (2003).

- [25] CMS Collaboration, CMS tracking performance results from early LHC operation, *Eur. Phys. J. C* 70 (2010) 1165. [arXiv:1007.1988](#), [doi:10.1140/epjc/s10052-010-1491-3](#).
- [26] CMS Collaboration Tracker Group, The CMS phase-1 pixel detector upgrade, *JINST* 16 (2021) P02027. [arXiv:2012.14304](#), [doi:10.1088/1748-0221/16/02/P02027](#).
- [27] CMS Collaboration, Description and performance of track and primary-vertex reconstruction with the CMS tracker, *JINST* 9 (2014) P10009. [arXiv:1405.6569](#), [doi:10.1088/1748-0221/9/10/P10009](#).
- [28] K. Rehermann, B. T. Tweedie, Efficient identification of boosted semileptonic top quarks at the LHC, *JHEP* 03 (2011) 59. [arXiv:1007.2221](#), [doi:10.1007/jhep03\(2011\)059](#).
- [29] V. Khachatryan, et al., Search for heavy stable charged particles in pp collisions at $\sqrt{s} = 7$ TeV, *JHEP* 03 (2011) 024. [arXiv:1101.1645](#), [doi:10.1007/JHEP03\(2011\)024](#).
- [30] CMS Collaboration, Search for heavy long-lived charged particles in pp collisions at $\sqrt{s} = 7$ TeV, *Phys. Lett. B* 713 (2012) 408. [arXiv:1205.0272](#), [doi:10.1016/j.physletb.2012.06.023](#).
- [31] V. Khachatryan, et al., Search for long-lived charged particles in proton-proton collisions at $\sqrt{s} = 13$ TeV, *Phys. Rev. D* 94 (2016) 112004. [arXiv:1609.08382](#), [doi:10.1103/PhysRevD.94.112004](#).
- [32] CMS Collaboration, Searches for long-lived charged particles in pp collisions at $\sqrt{s} = 7$ and 8 TeV, *JHEP* 07 (2013) 122. [arXiv:1305.0491](#), [doi:10.1007/JHEP07\(2013\)122](#).
- [33] R. A. Fisher, On the interpretation of χ^2 from contingency tables, and the calculation of p, *J. Roy. Stat. Soc.* 85 (1922) 87. [doi:10.2307/2340521](#).
- [34] S. Baker, R. D. Cousins, Clarification of the use of chi-square and likelihood functions in fits to histograms, *Nucl. Instrum. Meth.* 221 (1984) 437. [doi:10.1016/0167-5087\(84\)90016-4](#).

- [35] T. Junk, Confidence level computation for combining searches with small statistics, *Nucl. Instrum. Meth. A* 434 (1999) 435. [arXiv:hep-ex/9902006](#), [doi:10.1016/S0168-9002\(99\)00498-2](#).
- [36] A. L. Read, Presentation of search results: the CL_s technique, *J. Phys. G* 28 (2002) 2693. [doi:10.1088/0954-3899/28/10/313](#).
- [37] G. Cowan, K. Cranmer, E. Gross, O. Vitells, Asymptotic formulae for likelihood-based tests of new physics, *Eur. Phys. J. C* 71 (2011) 1554. [arXiv:1007.1727](#), [doi:10.1140/epjc/s10052-011-1554-0](#).
- [38] CMS Collaboration, The CMS statistical analysis and combination tool: COMBINE, submitted to *Comput. Softw. Big Sci.* (in press) (2024). [arXiv:2404.06614](#), [doi:10.1007/s41781-024-00121-4](#).